Advanced flutter simulation of flexible bridge decks

Gergely Szabó*[1], József Györgyi[1] and Gergely Kristóf[2]

[1]Department of Structural Mechanics, Budapest University of Technology and Economics, Hungary
[2]Department of Fluid Mechanics, Budapest University of Technology and Economics, Hungary

Abstract. In this paper a bridge flutter prediction is performed by using advanced numerical simulation. Two novel approaches were developed simultaneously by utilizing the ANSYS v12.1 commercial software package. The first one is a fluid-structure interaction simulation involving the three-dimensional elastic motion of a bridge deck and the fluid flow around it. The second one is an updated forced oscillation technique based on the dynamic mode shapes of the bridge. An aeroelastic wind tunnel model was constructed in order to validate the numerical results. Good agreement between the numerical results and the measurements proves the applicability of the novel methods in bridge flutter assessment.

Keywords: bridge deck flutter; fluid-structure interaction (FSI); modal derivatives method

1. Introduction

In the past decades really slender bridges have been built. Wind sensitivity of such buildings are well known, therefore their profound dynamic calculation due to wind loading is essential. There are several methods available in literature to calculate the critical flutter wind speed; basically wind tunnel test are used (Brownjohn *et al.* 2001, Gu *et al.* 2004, Larsen and Wall 2011) but CFD (Computational Fluid Dynamics) is increasingly taken as a mean in wind engineering (Szabó and Györgyi 2009, Zhiwen *et al.* 2008). Such techniques consider a section of the whole bridge deck only, irrespective of the highly complicated three-dimensional fluid-structure interaction phenomenon, which can lead to inaccuracies in the calculated critical wind speed. On top of all, the section modelling needs simplified mathematical models of the bridge deck that are not easy to make in some cases; there are complex bridge geometries, where the cross section is not constant along the bridge axis for instance, or a construction stage is to be modelled when the bridge is semi-finished. In such complicated cases full aeroelastic test are performed (King *et al.* 2011, Kim *et al.* 2011, Xu *et al.* 2011, Zhu *et al.* 2011).

The main goal of this paper is to give alternatives to the costly aeroelastic wind tunnel models by using advanced three-dimensional numerical simulations. In the past decade the fluid-structure interaction (FSI) simulation became an intensively studied field in engineering, ranging from bio-mechanical applications to wind engineering (Szabó and Kristóf 2010, Tezduyar *et al.* 2008). FSI simulation involving the three-dimensional elastic motion of a bridge deck, however, is rare in

---

* Corresponding author, Ph.D. Student, E-mail: hoeses@freemail.hu

literature, aircraft wings as elastic beams are studied this way mainly (Cavagna *et al.* 2007, Kamakoti *et al.* 2004, Wand and Lin 2008). Therefore, the authors of this paper have been developing the methodology of bridge deck flutter calculation with special focus on the three-dimensional coupling of the elastic mechanical motion and the fluid flow around the bridge deck (Szabó and Györgyi 2009, Szabó and Kristóf 2010).

In this paper the development of the methodology of an advanced FSI flutter simulation by utilizing ANSYS v12.1 commercial software will be presented. As a first step an aeroelastic wind tunnel model setup is introduced especially dedicated to the accurate validation of the FSI simulation. The ways of setting up the CFD and the mechanical FEM models are detailed that are necessary for the FSI simulation. Several aspects of the CFD simulation are covered with special focus on the optimal design of the computational mesh, the choice of the turbulence models as well as the time steps. As an FSI simulation is computationally expensive yet, the 3D CFD mesh was optimized in order to reduce the cell number used.

The FEM model of the bridge was carefully adjusted in order to provide the same structural properties as the wind tunnel model. The CFD and FEM models are automatically coupled by the ANSYS multi-field solver. The deformation of the CFD mesh around the deformed bridge deck is also handled by the dynamic mesh facility of the solver. The development of flutter was accelerated by using initial perturbation in the numerical solution. The FSI simulation was performed at several wind speeds until the critical value was found.

As a spin-off of the FSI studies, an elegant new method was also developed for bridge flutter study, which is based on the classical flutter calculation process. In this new approach the 3D CFD mesh was used that was applied for the FSI simulations too. The bridge boundary was given a forced oscillation according to the relevant dynamic mode shapes of the bridge model. The classical mathematical formulations for bridge flutter prediction were modified in order to be compatible with this new method.

The final goal in flutter calculation is the critical wind speed, which was determined by using four different methods; a wind tunnel test was carried out, the classical theory was applied and two novel approaches were developed. The first one is an FSI simulation, the second one is an updated forced oscillation technique, which is referred to as modal derivatives method later. The measured and calculated critical wind speeds showed good agreement; therefore the novel methods prove to be appropriate for bridge deck flutter assessment. Although simplified bridge geometry and uniform airflow were considered only, the newly developed methods can be adequate to handle arbitrary geometry combined with turbulent flow, provided that the proper computational background is available.

2. Introduction of the aeroelastic wind tunnel model

2.1 Design and fabrication of the aeroelastic wind tunnel model

In Fig. 1 the fully aeroelastic wind tunnel model is shown that was constructed in order to validate the numerical solutions. This model is an individual mechanical system for validation only and is not a scaled model of any real bridge structure. The bridge is made up by using an aluminum core beam, on which balsa elements are fixed. The cross section can be seen in Fig. 2. The contour of the model represents an idealized streamlined boxed bridge deck cross section (Larsen 2011).
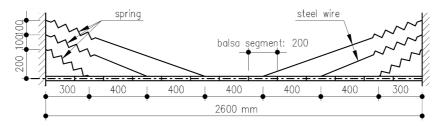
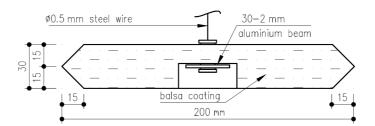Fig. 1 Side view of the aeroelastic wind tunnel model

Fig. 2 Cross section of the aeroelastic model

Fig. 3 The bridge model mounted in the wind tunnel

This section was chosen because it was believed to be handled properly with simpler turbulence models and coarse CFD mesh that is important to make the FSI simulation feasible. The core beam is fully constrained at both ends. There are six steel wires working like stay cables. These wires were softened by introducing spring elements (stiffness is 230 N/m) in order to make the bridge more flexible. The model can be seen in Fig. 3. The elastic modulus of the aluminum is 6.90E10 N/m², the density is 2620 kg/m³. The density of the balsa coating is 123 kg/m³.

At the middle balsa element of the bridge, at both sides of the segment, two piezoelectric accelerometers were fixed for monitoring the vertical motion. For the wind-off case the natural frequencies and logarithmic decrement values were measured. The first vibration mode was a symmetrical heave motion of the bridge deck with a natural frequency of 1.62 Hz. For the flutter analysis the first torsion mode is dominant, which was the fifth one with a natural frequency of 5.55 Hz. The logarithmic decrement for this mode was $\delta = 0.02$. These parameters were used for tuning the mechanical FEM model. During the measurement the wind speed was increased step by step. The high frequency vibrations caused by vortex shedding were ignored and the flutter phenomenon was only considered. The tests were done under low turbulence level.

3. Aerodynamic models of the bridge

3.1 Two-dimensional mesh of the investigated cross section

In classical flutter calculations the flutter derivatives are to be determined by considering a section of the bridge deck only (Brownjohn *et al.* 2001, Gu *et al.* 2004). These derivatives are found in the wind excitation forces in Eqs. (1) and (2).

$$F(t) = \frac{1}{2}\rho U^2 B \left[KH_1^*(K)\frac{\dot{h}(t)}{U} + KH_2^*(K)\frac{B\dot{\alpha}(t)}{U} + K^2H_3^*(K)\alpha(t) + K^2H_4^*(K)\frac{h(t)}{B} \right] \quad (1)$$

$$M(t) = \frac{1}{2}\rho U^2 B^2 \left[KA_1^*(K)\frac{\dot{h}(t)}{U} + KA_2^*(K)\frac{B\dot{\alpha}(t)}{U} + K^2A_3^*(K)\alpha(t) + K^2A_4^*(K)\frac{h(t)}{B} \right] \quad (2)$$

In Eqs. (1) and (2) F and M are the lift force and moment respectively. B is the width of the bridge deck, U is the inflow velocity, ρ is the air density, h and α are the vertical and rotational motion amplitudes respectively, ω is the oscillating circular frequency. $K = (B \cdot \omega)/U$ is the reduced frequency. Most commonly the reduced velocity ($U_{red} = U/(B \cdot f)$, f is the frequency) is used. It can be seen that the forces can be written as a function of the reduced frequency, the oscillating amplitudes and the $H1^*$-$H4^*$ and $A1^*$-$A4^*$ flutter derivatives.

Before setting up the three-dimensional coupled simulation, a two-dimensional CFD calculation was performed in order to determine the flutter derivatives for this cross section. The ANSYS-FLUENT was utilized in this case. The numerical mesh around the bridge contour can be seen in Fig. 4. The height of the computational domain is 2.40 m, the velocity inlet boundary was 1.00 m left from the bridge centre, the outflow boundary was 1.40 m right. At the top and bottom planes symmetry boundary conditions were used.

The flutter derivatives were extracted by means of forced vibration method (Larsen 2011). The bridge deck is to be given a vertical and a rotational motion at different reduced wind velocities. During the simulation the acting lift forces and moments can be recorded from which the flutter derivatives can be extracted by using Eqs. (1) and (2). The oscillation frequency was constant (6.00 Hz), while the inflow velocity was incrementally increased. The lift motion amplitude was set to 20 mm, the rotation angle amplitude was 0.1744rad. The applied cell number was 12590. The k-ε turbulence model was chosen, because it is one of the best turbulence model in terms of convergence. Moreover turbulence is of minor importance in case of streamlined cross sections in forced oscillations according to the authors' numerical experiences in this field.
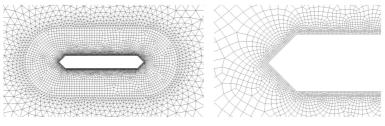

Fig. 4 Two-dimensional numerical mesh around the bridge deck
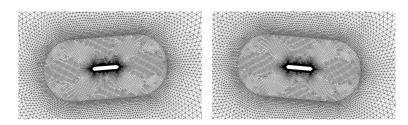
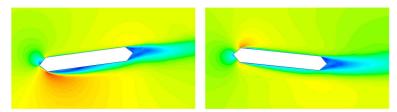Fig. 5 Rotated bridge deck at two different phases

Fig. 6 Velocity contour plot around the rotated bridge deck

The motion of the wall domain of the bridge needs the deformation of the numerical mesh, which can be assured by using the dynamic mesh option of the solver. The mesh deformation was relatively low, so there was no need to implement re-meshing technique, instead a smoothing mesh deformation was enough to handle the bridge deck motion. The bridge contour is surrounded by a special mesh region that is rigidly moving with the bridge. Thus, the good mesh quality can be preserved in the vicinity of the bridge, which is essential for good numerical results. In order to further reduce numerical errors, rectangular cells are used in this "bubble" region. Outside of the rigid body mesh, however, triangular cells were applied that are very adequate to handle the motion of the bridge. The mesh deformation is based on a spring analogy, where the mesh edges work like linear springs. Thus, the majority of the total cell deformation occurs at the larger triangular cell region where the longest mesh edges as springs suffer the greatest strain. In Fig. 5 two rotated phases are shown. Apparently the triangular cells are not distorted unpleasantly.

In the URANS (Unsteady Reynolds-Averaged Navier-Stokes simulation) simulation the time step was set to 0.00001s. Thus, the Courant-number was set below 1 for the whole computational domain even at the highest wind velocity ($U = 24$ m/s), that is the fluid does not move longer than a cell size in a time step. The end time was 0.5s, the total number of time steps was $N = 50.000$. By performing URANS simulation for both vertical and rotational motion, the flutter derivatives were extracted within a certain reduced velocity range (4, 8, 12, 16 and 20). The belonging wind velocities were $U = 4.80$, 9.60, 14.40, 19.60 and 24.00 m/s respectively. The velocity contour plot can be seen in Fig. 6 in case of rotational motion. The above presented two-dimensional simulation was preformed by using fine mesh and time stepping, thus accurate flutter derivatives values can be expected.

3.2 CFD model for the three-dimensional fluid-structure interaction simulation

The FSI and the modal derivatives method requires three-dimensional CFD mesh around the investigated bridge boundary. As the cell number of a 3D mesh with the same density is much larger than that of a 2D mesh, the computational efforts are also higher. It is essential therefore to reduce the

Gergely Szabó, József Györgyi and Gergely Kristóf
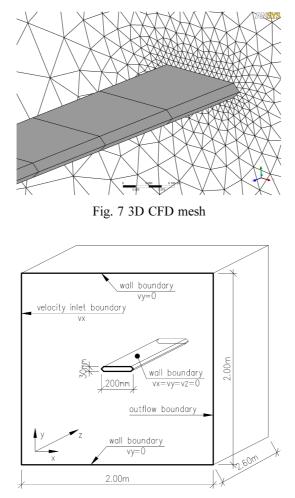

Fig. 7 3D CFD mesh

Fig. 8 Computational domain and the boundary conditions

number of cells used in order to make the simulations feasible. The ANSYS-CFX was utilized in this case. In Fig. 7 the applied mesh is shown. It can be seen that much coarser mesh is used than the 2D mesh (Fig. 4). The total number of cells was reduced to 49.816, therefore the computational time is acceptable. A time step of 0.0008s was used. The bridge boundary was subdivided into 13 parts along the bridge axis resulting in 13 parts in accordance with the aeroelastic model (Fig. 1).

In case of two-dimensional meshes an efficient meshing strategy has been worked out that can provide fine mesh quality throughout the whole unsteady computational process (Fig. 5). At a three-dimensional mesh a rigid surrounding mesh region cannot be defined as the fully spatial motion cannot be restrained. This means a little deformation of the boundary layer cells. The deformation of the cells near the bridge deck boundary can be restricted by applying different spring stiffness for the mesh smoothing; the spring stiffness is not constant, but increases near the boundary layer region. By setting the mesh deformation this way, the deformation of the boundary layer cells is insignificant.

The *k-ε* model was chosen to model turbulence, as in case of the 2D simulations. At the inlet a velocity inlet, at the outlet the outflow boundary conditions were used. At the top and bottom planes

symmetry conditions, at the both sides wall boundary conditions with free slip constraint were applied. On the whole bridge surface wall boundary was used. The computational domain can be seen in Fig. 8.

The three-dimensional mesh can be used in the FSI simulation or in the modal derivatives method, which will be introduced later. It is essential in both cases that the aerodynamic forces are calculated accurately in order to determine the critical wind speed precisely. Before using the 3D mesh it was necessary to ascertain about its accuracy, as coarse mesh and large time step were used in order to reduce the computational time. The ANSYS-CFX enables the user to define arbitrary motions of the bridge boundary; therefore two types of spatial motions were defined; translational and rotational ones. In Fig. 9 a rotated geometry is shown. It can be seen that the good mesh quality is preserved throughout the whole simulation as in case of the 2D simulation.

The maximal amplitudes at the middle of the bridge deck are the same as in case of the 2D simulations. The same reduced velocity range (4, 8, 12, 16 and 20) was considered. The lift force and moment signals on the middle 20 cm long section were used to extract the flutter derivatives. In Fig. 10 the flutter derivatives extracted from the 2D and 3D models are shown. The analytical results for the ideal flat plate case are also illustrated (Theodorsen 1935). It can be seen that the numerical results are close together indicating that the 3D model can be used for the FSI and the modal derivatives method. In case of the most important $H3^*$, $A2^*$ and $A3^*$ derivatives, the coincidence is excellent.

The flutter derivatives give a good understanding of the flutter performance of bridge decks by purely observing their shape, especially that of the $A2^*$ derivative. As the $A2^*$ is the multiplier of the angular velocity of the bridge deck in Eq. (2), it has a major role in the flutter equation. If $A2^*$ is negative, the torsion motion gives a positive damping to the structure in the fluid flow, consequently hinders the development of flutter. If it turns to be positive, the damping of the torsion mode is negative, which decreases dramatically the flutter speed. In the case of the investigated cross section the $A2^*$ is negative at all reduced wind speed, therefore it is considered to be a streamlined cross section. As a consequence, the flutter derivatives of streamlined bridge decks are close to that of a flat plate (Fig. 10).

In this chapter the methodology of constructing a 3D CFD mesh for bridge flutter simulation was shown. It was highlighted that the cell number is important to be kept low; therefore a comparison with the results of a 2D CFD model was made. By using this optimization, the 3D mesh can be accurate and contain low number of cells in the same time.
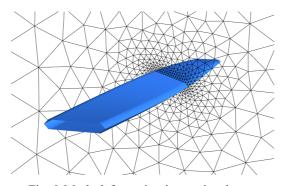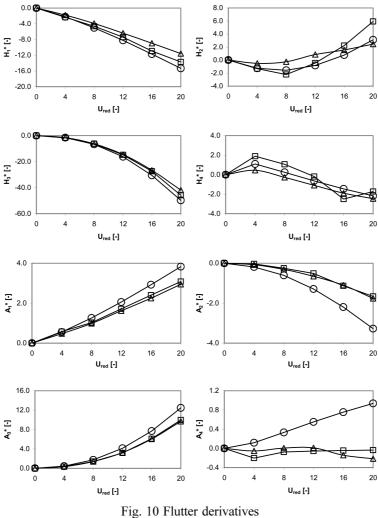

Fig. 9 Mesh deformation in rotational case

Fig. 10 Flutter derivatives
Circle: Flat plate theory, Rectangle: CFD_2D, Triangle: CFD_3D

4. Mechanical models of the bridge

4.1 Three-dimensional beam model

In order to perform a fluid-structure interaction simulation the structural dynamics model of the bride is also necessary to make. The mechanical model is made up by using the ANSYS mechanical classic module that can be seen in Fig. 11. The aluminium beam and the balsa elements are modelled with BEAM4 spatial beam elements with 6DOFs per each of the two nodes. The cable elements are modelled with LINK8 spatial link element that is capable of handling tension-compression forces only. The ends of the aluminium beam and the cables are fully fixed. The dynamical mode shapes and natural frequencies are shown in Fig. 12.
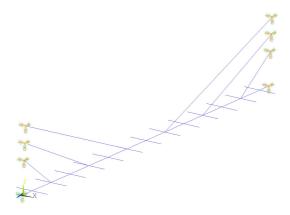
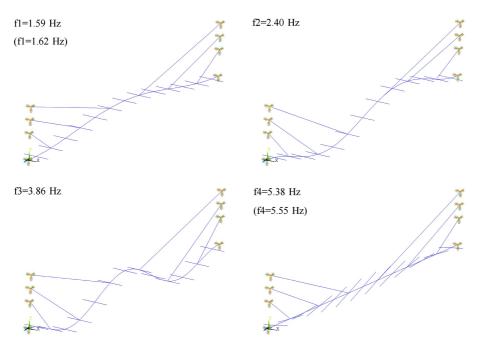Fig. 11 Mechanical beam model of the aeroelastic wind tunnel model

f1=1.59 Hz

(f1=1.62 Hz)

f2=2.40 Hz

f3=3.86 Hz

f4=5.38 Hz

(f4=5.55 Hz)

Fig. 12 Dynamic mode shapes and natural frequencies of the beam model (measured values in parenthesis)

4.2 3D shell model

For the traditional flutter calculation a beam model may provide accurate results as to the mode shapes and natural frequencies. In case of an advanced three-dimensional coupled fluid-structure simulation an FEM model by using shell element is essential. In ANSYS 12.1 the coupling of structural mechanics and fluid mechanics is handled automatically. The most important step is the definition of an interaction interface on which the communication between the FEM mesh and the CFD mesh is done. It was obvious that this surface was the boundary of the bridge. In Fig. 13 the FEM model can be seen. The main difficulty was the determination of the mechanical properties; the shell model has to behave as the aeroelastic wind tunnel model, though there is no core beam

and cross balsa beams in this case, as it is a continuum. To overcome this problem, the surface elements were given proper thickness and elastic modulus in order to provide the same stiffness as the beam model. At first the torsion rigidity was tuned by using the expression below Eq. (3).

$$I_t G = \frac{4A^2 t}{K} \frac{E}{2(1+\nu)} \tag{3}$$

In Eq. (3) I_t is the torsion inertia, G is the shear modulus, A and K are the area and the perimeter of the cross section, respectively, E is the elastic modulus, ν is the Poisson-ratio. The t thickness of the boundary shell elements was set to 0.004 m. E and ν values were fixed so as to obtain the same torsion frequency as the beam model. After that E and ν were changed slightly in order to approximate the first natural frequency of the beam model. The final parameters are $E = 3.874E6$ N/m² and $\nu = 0.31$.

It is obvious that the shell element cannot have real material properties as a large boxed section has to provide same stiffness as an aluminium core beam. As a consequence the flexural stiffness of the boundary is really low, therefore extremely vulnerable to normal forces due to the airflow pressure. To overcome this problem, volume elements were introduced to fill the boxed tube. The mechanical properties were chosen in order not to affect the longitudinal behaviour; these volume elements have stiffness normal to the surface only. By using this technique the surface was stiffened properly, preventing it from being deformed locally.

The filling volume elements were given the density of the balsa elements. Additional masses like the weight of the aluminium core beam and the bolts were taken into account by modifying the density. The cables were defined the same as in case of the beam model. In dynamic calculation damping is of primary importance. In the FSI simulation the Raleigh damping can only be used in ANSYS, which is problematic as the structural damping can be modelled by using frequency-independent damping precisely. By using the Raleigh constants, however, the required percentage damping can be approximated. The logarithmic decrement of damping of the torsion vibration mode was $\delta = 0.02$. The percentage damping is then $\xi = \delta/2\pi = 0.0032$. This value is targeted by setting α and β damping constants according the equation $\alpha + \beta\omega_i = 2\omega_i\xi$ for the desired i_{th} ω_i circular natural frequencies. In Fig. 14 the targeted and the achieved values are shown. The damping of the model is really close to the designed value in the 4-5 Hz range that is expected to be important for
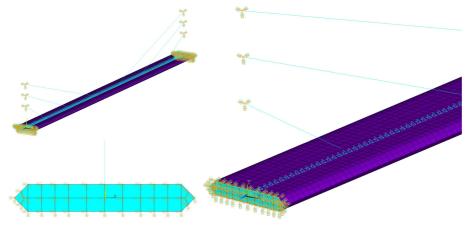

Fig. 13 Mechanical FEM model of the aeroelastic wind tunnel model

Fig. 14 Percentage damping of the wind tunnel model and the shell FEM model

f1=1.68 Hz
(f1=1.62 Hz)

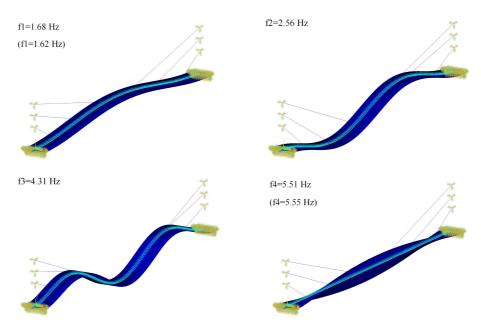f2=2.56 Hz

f3=4.31 Hz

f4=5.51 Hz
(f4=5.55 Hz)

Fig. 15 Dynamic mode shapes and natural frequencies of the shell model (measured values in parenthesis)

flutter phenomenon. Below 3 Hz the damping of the model differs from the constant 0.0032 value. It is important to underline, however, that in case of flutter the role of damping is of minor importance. In Fig. 15 the calculated mode shapes and natural frequencies are shown.

5. Calculation of the critical wind speed

The final aim in case of a flutter simulation of a bridge structure is the determination of the critical wind speed. The critical wind speed was calculated by using four different techniques; direct measurement of the wind tunnel model, three-dimensional FSI simulation, a classical approach by using the flutter derivatives and a novel approach by using newly developed modal derivatives based on three-dimensional forced vibration technique with CFD simulation. These four methods are introduced in the four sections as follows.
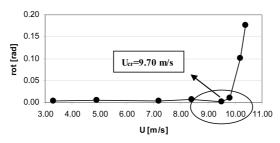
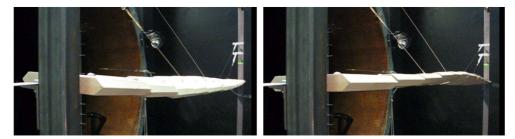Fig. 16 Rotation amplitude as a function of the inflow wind speed

Fig. 17 Deformed bridge deck at the speed of 10 m/s

5.5.1 Wind tunnel measurements

The aeroelastic wind tunnel model was equipped with two accelerometers on both sides of the middle balsa member, therefore vertical and torsion motion accelerations were measured. By filtering and integrating the acceleration signals the motion amplitudes were determined. The wind speed was varied from 3 up to 10.4 m/s. The rotation amplitudes versus wind velocity curve can be seen in Fig. 16. It can be seen that the motion amplitude remains moderate below 9 m/s. From 9.5 m/s the amplitudes are growing rapidly. The wind velocity during the measurement was limited to 10.4 m/s as the motion amplitudes were extremely high. The critical wind speed was extrapolated at 9.7 m/s by using the last three data points where the amplitudes are growing definitely (see Fig. 16).

At the speed of 10 m/s the deformed bridge deck is illustrated in Fig. 17. The flutter phenomenon is fully developed in this case. It can be clearly seen that the bridge deck is in a spatial rotation state.

5.5.2 Three-dimensional FSI simulation

To setup an FSI simulation both fluid and mechanical models are necessary. The CFD and the FEM models have already been introduced. Once these two models are made, the FSI simulation can be carried out. The coupling process is completely handled by ANSYS with the built-in multi-field solver. The solution process is a transient dynamic calculation as to the structural part. The CFD solver uses an unsteady finite volume method. The global time step is 0.0008s, in accordance with the CFD model. At each time step the solver does a mapping process that is passing the FEM node deformation to the CFD mesh and the pressure forces from the CFD simulation to the FEM model. Then the CFD mesh is deformed and the field variables are calculated. The deformation of the FEM model is also calculated due to the pressure forces. This process is repeated in a so called "stagger" iteration until the norm of the interface load change vector is smaller than a tolerance value. Once convergence is reached, the solver proceeds to the next time step.

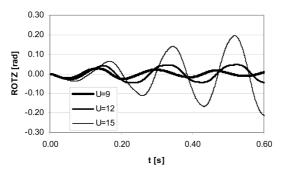The initial condition is a delicate issue in a coupled simulation. In the CFD setup constant wind

Fig. 18 Rotation of the middle section of the bridge at different wind speeds
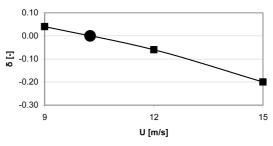

Fig. 19 Interpolation of the critical wind speed

speeds were defined at the velocity inlet boundary condition. As in case of the wind tunnel test, several wind speeds were defined in order to find the critical wind speed. In case of a coupled simulation the development of flutter needs lot of computational time, therefore it is not feasible to start from a zero-deformation condition. Instead, in order to fasten the simulation, a constant torsion moment was given to the bridge deck within the first 20 time steps as a perturbation. The bridge deck is taking a flutter-like shape until the end of the 20 time steps and then the simulation continues without additional moment. From the initial 20 time steps the model is deformed enough to generate self-excited forces on itself. With the increase of the wind speed the damping of the bridge deck oscillation decreases, and vanishes over 10 m/s (see Figs. 18 and 19).

The rotation amplitude decreases at the wind speed of 9 m/s (Fig. 18). At 12 m/s already slightly grows and at 15 m/s the growth is remarkable. As in case of the wind tunnel measurement, the critical wind speed is approximated by interpolation (see Fig. 19). The critical wind speed by using the FSI simulation is 10.2 m/s. The deformed bridge deck with the streamlines around it can be seen in Fig. 20 at four different time steps. The bridge deck has a typical spatial deformation that is usual in case of the so-called coupled flutter; the presence of the torsion and a heave motion is dominant. In this case the fourth (torsion) and the first (heave) mode shapes can be recognized. These two modes are coupled in a flutter motion. The motion of the bridge deck dominates the flow-field around it, and the flow field generates unsteady forces on the bridge deck as a consequence. This mutual interaction is responsible for the flutter phenomenon. In Fig. 21 the deformed FEM mesh can be seen without the CFD results. A simulation belonging to a certain wind speed required about 8 days computational time [Intel Quad Q6600 2.40 GHz, four core, RAM: 8Gb]. The time step was 0.0008s, and the end time was 0.8s. This is the reason for performing as few wind speed cases as possible.
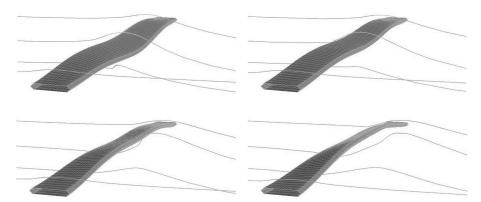
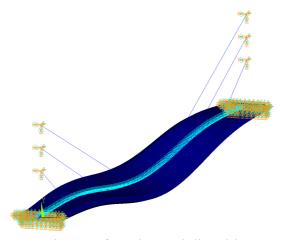Fig. 20 Streamlines around the deformed bridge deck at four different time steps

Fig. 21 Deformed FEM shell model

5.5.3 Classical approach

In traditional flutter prediction techniques the flutter derivatives are calculated by using either wind tunnel tests or CFD simulations. These procedures consider a section of the whole bridge deck only. The mathematical formulations are presented according to Starossek (1997). This method was worked out for a 2DOF dynamic system with translational and rotational degrees of freedoms. On the right side of Eq. (4) the wind generated force vector appears. In Eq. (4) M: mass matrix, C: damping matrix, K: stiffness matrix, x: displacement vector that contains the vertical and torsion motions. Q load vector contains the lift force and moment that are detailed in Eqs. (1) and (2).

$$M\ddot{x} + C\dot{x} + Kx = Q = \begin{bmatrix} F \\ M \end{bmatrix} \qquad (4)$$

By using the formula Eq. (5) below, the Q vector can be rewritten as Eqs. (6) and (7). In Eq. (5) ω is the unknown circular frequency, $i = \sqrt{-1}$ is the complex unit.

$$x = \tilde{x}e^{i\omega t} = \begin{bmatrix} \tilde{h} \\ \tilde{\alpha} \end{bmatrix} e^{i\omega t} \qquad (5)$$

$$F = \rho U^2 b^2 \left[i\frac{2\omega^2}{U^2}H_1^*(K)\tilde{h} + i\frac{4b\omega^2}{U^2}H_2^*(K)\tilde{\alpha} + \frac{4b\omega^2}{U^2}H_3^*(K)\tilde{\alpha} + \frac{2\omega^2}{U^2}H_4^*(K)\tilde{h} \right] \quad (6)$$

$$M = \rho U^2 b^2 \left[i\frac{4b\omega^2}{U^2}A_1^*(K)\tilde{h} + i\frac{8b^2\omega^2}{U^2}A_2^*(K)\tilde{\alpha} + \frac{8b^2\omega^2}{U^2}A_3^*(K)\tilde{\alpha} + \frac{4b\omega^2}{U^2}A_4^*(K)\tilde{h} \right] \quad (7)$$

The flutter derivatives constitute the following terms Eq. (8). These terms are used by Starossek (1997). As the flutter derivatives are functions of the reduced frequency or the reduced velocity, the c_{ii} expressions will also be functions.

$$c_{hh} = \frac{2}{\pi}H_4^* + i\frac{2}{\pi}H_1^*$$

$$c_{h\alpha} = \frac{4}{\pi}A_4^* + i\frac{4}{\pi}A_1^*$$

$$c_{\alpha h} = \frac{4}{\pi}H_3^* + i\frac{4}{\pi}H_2^*$$

$$c_{\alpha\alpha} = \frac{8}{\pi}A_3^* + i\frac{8}{\pi}A_2^* \quad (8)$$

By using Eqs. (8), (6) and (7) yields Eqs. (9) and (10), and finally providing L force matrix Eq. (11).

$$F = \omega^2 \rho \pi b^2 (c_{hh}\tilde{h} + bc_{h\alpha}\tilde{\alpha}) \quad (9)$$

$$M = \omega^2 \rho \pi b^2 (bc_{\alpha h}\tilde{h} + b^2 c_{\alpha\alpha}\tilde{\alpha}) \quad (10)$$

$$L = \rho \pi b^2 \begin{bmatrix} c_{hh} & bc_{h\alpha} \\ bc_{\alpha h} & b^2 c_{\alpha\alpha} \end{bmatrix} \quad (11)$$

By assuming the damping matrix as below Eq. (12), the Eq. (4) matrix differential-equation yields Eq. (13). The q load vector includes the L matrix, and the unknown oscillating frequency. In Eq. (12) $\gamma = 2\xi$ is the damping parameter.

$$C = \frac{\gamma}{\omega}K \quad (12)$$

$$M\ddot{x} + (1 + i\gamma)Kx = q \quad (13)$$

$$q = \omega^2 L\tilde{x} \quad (14)$$

Finally, the Eq. (15) equation has to be investigated in terms of stability. The nontrivial solution can be found according to the Eq. (16) eigenvalue problem.

$$\{(1 + i\gamma)K - \omega^2[M + L(U_{red})]\} \cdot \tilde{x} = 0 \quad (15)$$

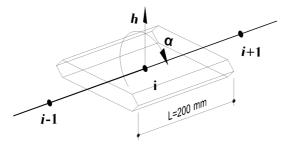$$\left|(1 + i\gamma)K - \omega^2[M + L(U_{red})]\right| = 0 \quad (16)$$

Fig. 22 A 200 mm long segment of the aeroelastic bridge model

The solution procedure is as follows; the U_{red} value is varied increasingly. At every single U_{red} value the Eq. (8) terms can be interpolated, and the complex ω frequency can be found, from which the logarithmic decrement of the system oscillating in airflow can be evaluated. If the damping vanishes, the critical U_{red} value is found, from which the critical U wind speed can be obtained. This method requires a 2DOF model of an ordinary structure, which is not necessarily easy to construct. By using the dynamic properties of the bridge deck of the 2DOF method can be developed. Consider the whole aeroelastic model as a set of 2DOF systems in Fig. 22.

The aeroelastic wind tunnel model can be regarded as a system with 13 nodes, as 13 balsa segments that are attached to the main beam. The Eq. (11) load matrix is rewritten as Eq. (17).

$$\boldsymbol{L} = \pi\rho b^2 \begin{bmatrix} c_{hh} & bc_{h\alpha} & & & \\ bc_{\alpha h} & b^2 c_{\alpha\alpha} & & & \\ & & \cdot & & \\ & & & \cdot & \\ & & & & c_{hh} & bc_{h\alpha} \\ & & & & bc_{\alpha h} & b^2 c_{\alpha\alpha} \end{bmatrix} \begin{matrix} n = 1 \\ n = 1 \\ \cdot \\ \cdot \\ n = 13 \\ n = 13 \end{matrix} \qquad (17)$$

In Eq. (17) the aeroelastic bridge is considered as a bridge deck with 13 nodes, with a lift force and a moment at each node. Therefore the size of the $\boldsymbol{L}$ matrix is 26×26 in this case. By seeking the solution in the form Eq. (18), and using expressions in Eq. (19), the Eq. (20) eigenproblem is to be solved now. The mode shapes and natural frequencies of the bridge deck are similarly exploited by Mishra *et al.* (2006) but instead of the frequency domain the time domain approach was applied by using rational functions. Starossek (1997), however, proposed the FEM approach without applying modal analysis.

$$\tilde{\boldsymbol{x}} = \boldsymbol{V}\tilde{\boldsymbol{y}} \qquad (18)$$

$$\boldsymbol{V}^T \boldsymbol{L} \boldsymbol{V} = \boldsymbol{A}, \quad \boldsymbol{V}^T \boldsymbol{M} \boldsymbol{V} = \boldsymbol{E}, \quad \boldsymbol{V}^T \boldsymbol{K} \boldsymbol{V} = \langle \omega_{0r}^2 \rangle \qquad (19)$$

$$\left| (1 + i\gamma)\langle \omega_{0r}^2 \rangle - \omega^2 [\boldsymbol{E} + \boldsymbol{A}(U_{red})] \right| = 0 \qquad (20)$$

In Eq. (18) $\boldsymbol{V}$ contains two column vectors belonging to the chosen mode shapes. In Eq. (19) $\boldsymbol{E}$ is the unity matrix, ω_{0r} is the r_{th} natural circular frequency of the bridge structure. The solution process

of the Eq. (20) system is the same as in case of a 2DOF system. On top of all, the size of the Eq. (20) in case of two mode shapes is also the same as that of the 2DOF system. It can be seen that if the flutter derivatives as functions are known for a certain bridge shape, the critical wind speed can be calculated for the bridge structure. This can be done by reducing the bridge into a 2DOF system or by using the mode shapes and natural frequencies in the framework of the modal analysis.

The main shortcoming of the above described method is that the three-dimensional flow field is reduced into a set of two-dimensional flows that is the flow parallel with the bridge axis is neglected. On top of all if the cross section is not constant along the bridge axis for instance, the flutter derivatives have to be determined at several cross sections, resulting in a tedious calculation process. In the next section the modal derivatives method is introduced, which can overcome the above mentioned shortcomings of the classical methods.

5.5.4 Modal derivatives method

In this section the advantages of the flutter derivatives theory and the three-dimensional CFD modelling are combined in order to develop a novel technique. The flutter condition is assumed to show harmonic motion; therefore the analysis is obvious to carry out in the frequency domain as in case of the classical flutter calculation. In Eq. (19) matrix A can be compiled easily, as L and V matrices are known for a certain fixed U_{red} value. In order to replace the two-dimensional CFD simulations with the advanced three-dimensional simulation, the A matrix should be examined in detail; after multiplying the L matrix by V matrix, A reads Eq. (21).

$$A = \pi \rho b^2 \begin{bmatrix} \sum_i v_{hi}^2 \cdot c_{hh} & b \cdot \sum_i v_{hi} \cdot v_{\alpha i} \cdot c_{h\alpha} \\ b \cdot \sum_i v_{hi} \cdot v_{\alpha i} \cdot c_{\alpha h} & b^2 \cdot \sum_i v_{\alpha i}^2 \cdot c_{\alpha\alpha} \end{bmatrix} \quad (21)$$

The elements of the A matrix are terms c_{ii} Eq. (8) multiplied by the elements of the mode shape vectors. The main goal is to compile the A matrix based on the result of the three-dimensional CFD simulation instead of the 2D ones. As mentioned earlier the ANSYS-CFX enables the user to define arbitrary motion of the bridge deck. The 3D CFD model was tested and the flutter derivatives were extracted by defining translational and rotational spatial deformation of the bridge boundary (see Figs. 9 and 10). The ways of prescribing this motion is explained here in detail. Obviously the first translational and rotational mode shapes were used (Fig. 23), as these contribute to the flutter motion.
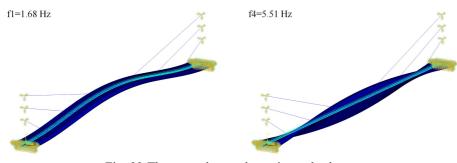
f1=1.68 Hz   f4=5.51 Hz
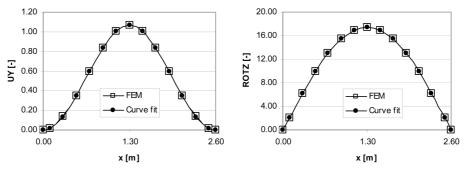
Fig. 23 The two relevant dynamic mode shapes

Fig. 24 Heave (UY) and torsion (ROTZ) mode shape values used for the calculation

It is necessary that the bridge boundary is given a predefined motion as a function of time and space. In Fig. 24 the discrete mode shape values of the FEM model are fitted by analytical functions. The motion in time is written by using harmonic function. The translational function of the bridge deck is written in Eq. (22), where the vertical position of every point (h) is defined at location (z) and at time (t). Likewise the rotation can be written as Eq. (23), from which vertical and horizontal components can be derived. The maximal translational amplitude at the middle of the deck is $h_0 = 20$ mm, the maximal rotational amplitude is $\alpha_0 = 0.1744$ (10°), as in case of the 2D model.

$$h(z, t) = [1 - cos(z2\pi/L)] \cdot h_0/2 \cdot sin(\omega t) \tag{22}$$

$$\alpha(z, t) = [sin(z\pi/L)] \cdot \alpha_0/2 \cdot sin(\omega t) \tag{23}$$

If the three-dimensional bridge deck is oscillated according to the certain mode shapes, the aerodynamic forces belonging to the i_{th} segment (see Fig. 22) can be calculated. There are 13 moment and 13 lift force signals at each simulation case. In Fig. 25 the moment signals are shown ($U_{red} = 8$) at $i = 1, 4$ and 7 sections.

Based on the aerodynamic forces and moments in relation with the modal oscillation, Eq. (21) equation can be rewritten as Eq. (24). The over hat denotes that the $\hat{A}$ matrix is written by using the mode shape vectors. The elements of matrix $\hat{A}$ can be compiled analogously as shown in Eq. (8), but instead of using the flutter derivatives of a 2D section of the bridge new terms are to be used. In Eq. (25) these new flutter derivatives are introduced, that are extracted based on the results of the modal oscillation of the 3D CFD model, therefore can be called as modal (flutter) derivatives. As the 3D bridge is oscillated according to the selected mode shape vectors, the resulting force and moment
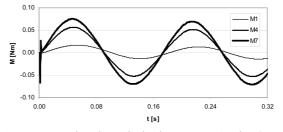

Fig. 25 Moment signals at deck element 1, 4 and 7 ($U_{red} = 8$)

signals at each i_{th} element of the bridge deck can be assumed to be proportional to the mode shape values at the same locations. Thus, the force and moment signals are to be multiplied by the mode shape values only at once, contrary to the case of the *A* matrix in Eq. (21). The summation in Eq. (21), thus, can be substituted by summing up the forces and moments multiplied by the relevant mode shape values at the i_{th} location.

$$\hat{A} = \pi\rho b^2 \cdot \begin{bmatrix} \hat{c}_{hh} & b \cdot \hat{c}_{h\alpha} \\ b \cdot \hat{c}_{\alpha h} & b^2 \cdot \hat{c}_{\alpha\alpha} \end{bmatrix} \tag{24}$$

$$\hat{H}_1^* = -U_{red}^2 \cdot \frac{max\left[\sum_i v_{hi} \cdot F_{hi}(t)\right]}{q \cdot B \cdot (2\pi)^2 \cdot (h_0/\hat{h})/B} sin(\beta) \qquad \hat{H}_2^* = -U_{red}^2 \cdot \frac{max\left[\sum_i v_{hi} \cdot F_{\alpha i}(t)\right]}{q \cdot B \cdot (2\pi)^2 \cdot (\alpha_0/\hat{\alpha})} sin(\beta)$$

$$\hat{H}_3^* = U_{red}^2 \cdot \frac{max\left[\sum_i v_{hi} \cdot F_{\alpha i}(t)\right]}{q \cdot B \cdot (2\pi)^2 \cdot (\alpha_0/\hat{\alpha})} cos(\beta) \qquad \hat{H}_4^* = U_{red}^2 \cdot \frac{max\left[\sum_i v_{hi} \cdot F_{hi}(t)\right]}{q \cdot B \cdot (2\pi)^2 \cdot (h_0/\hat{h})/B} cos(\beta)$$

$$\hat{A}_1^* = -U_{red}^2 \cdot \frac{max\left[\sum_i v_{\alpha i} \cdot M_{hi}(t)\right]}{q \cdot B^2 \cdot (2\pi)^2 \cdot (h_0/\hat{h})/B} sin(\beta) \qquad \hat{A}_2^* = -U_{red}^2 \cdot \frac{max\left[\sum_i v_{\alpha i} \cdot M_{\alpha i}(t)\right]}{q \cdot B^2 \cdot (2\pi)^2 \cdot (\alpha_0/\hat{\alpha})} sin(\beta)$$

$$\hat{A}_3^* = U_{red}^2 \cdot \frac{max\left[\sum_i v_{\alpha i} \cdot M_{\alpha i}(t)\right]}{q \cdot B^2 \cdot (2\pi)^2 \cdot (\alpha_0/\hat{\alpha})} cos(\beta) \qquad \hat{A}_4^* = U_{red}^2 \cdot \frac{max\left[\sum_i v_{\alpha i} \cdot M_{hi}(t)\right]}{q \cdot B^2 \cdot (2\pi)^2 \cdot (h_0/\hat{h})/B} cos(\beta)$$

$$\tag{25}$$

Finally, the maximum values of these functions are considered, as in case of the extraction of the classical flutter derivatives. If necessary, the summed force and moment functions can be filtered in order to remove the high frequency components that are irrelevant in flutter analysis. In Eq. (25) $\hat{h}$ and $\hat{\alpha}$ are the maximum values of the mode shape vectors (Figs. 23 and 24), respectively, β is the phase shift between the force or moment functions and the translational or rotational oscillations, $q = 0.5 \rho U^2$ is the dynamic pressure, where U is the flow speed, ρ is the air density. In Fig. 26 the streamlines around the rotated bridge deck are shown at two different time steps at $U = 9.60$ m/s.

Once the Eq. (25) modal derivatives are extracted in a necessary U_{red} range, the Eq. (24) $\hat{A}(U_{red})$ matrix is given as a function of the reduced velocity, and can be used instead of the *A* matrix in Eq.
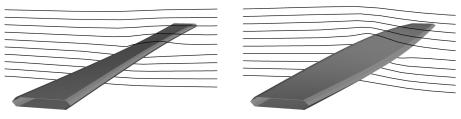

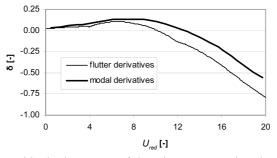Fig. 26 Streamlines around the rotated bridge deck at $U = 9.60$ m/s

Fig. 27 Logarithmic decrement of damping versus reduced wind speed

(20), therefore the solution of the eigenproblem does not need more computational efforts. In Fig. 27 the damping of the rotation mode can be seen as a function of the reduced velocity by using the flutter derivatives and the modal derivatives method. The critical wind speed can be evaluated from the critical reduced wind speed. The critical wind speed is 9.2 m/s by using the $\hat{A}$ matrix in the modal derivatives method, and 8.7 m/s by using the A matrix based on the 2D flutter derivatives and the mode shape vectors. The modal derivatives were extracted at five U_{red} values resulting in 10 simulation cases, which require approximately 10 days computational time (same computer as in case of the FSI).

6. Conclusions

The conclusions of this paper are drawn as follows:

· It was found that bridge flutter assessment by using three-dimensional coupled simulation is missing from literature, which would be desirable, as in case of long-span bridges or special structural systems precisely designed full aeroelastic wind tunnel models are performed that are costly, nevertheless.
· The methodology of performing a three-dimensional FSI simulation for bridge flutter study by utilizing ANSYS v12.1 commercial software package was presented. The challenges of constructing the CFD and FEM models as well as optimizing the meshes and time stepping were introduced. It was shown that even a coarse CFD mesh can be adequate to give accurate aerodynamic forces for a streamlined bridge deck, which is essential to make the FSI simulation feasible. The simulation was accelerated by introducing an initial geometrical perturbation. The FSI simulation provided realistic three-dimensional flutter-deformation of the bridge deck, which was a great achievement as it can not be found in literature yet.
· As an alternative to the FSI simulation an elegant new method was also developed. The CFD mesh and the dynamic properties of the bridge were necessary. The CFD mesh was given a 3D forced oscillation according to the relevant mode shapes of the bridge deck. The classical flutter derivatives theory was modified and new terms, the modal derivatives are proposed instead. The critical wind speed calculation can be simply performed as in case of the classical method.
· The two novel approaches were validated by using a full-aeroelastic wind tunnel model. The measured critical wind speed was 9.7 m/s. The FSI and the modal derivatives method gave a critical wind speed of 10.2 m/s and 9.2 m/s, respectively, which is considered to be excellent

agreement, proving their applicability in flutter prediction. The classical method based on the 2D flutter derivatives gave a value of 8.7 m/s, which is the lowest among all the presented methods.

• Comparing the two novel approaches both can be proposed to flutter prediction, but they are different in manner. The FSI simulation is a coupled fluid-structure interaction simulation that models the free oscillation vibration of the bridge deck in fluid flow, involving the dynamic properties of the bridge. The critical wind speed can be then established by analysing the motion at different wind speeds. To the contrary, the modal derivatives method assumes harmonic motion that simplifies the problem as it can be handled in the frequency domain. The FSI simulation is more universal, it can be used for many kinds of wind loading problems, such as buffeting, vortex shedding or galloping as well. Even more, structural nonlinearities can also be included in the simulation. If the flutter prediction of a linear structure is to be investigated, however, the modal derivatives method is proposed, as requires less computational time. Although the proposed methods were developed considering simplified bridge geometry and flow field, they can be extended to complex bridge geometries and turbulent wind flow conditions.

Acknowledgments

References

Brownjohn, J.M.W. and Choi, C.C. (2001), "Wind tunnel section model study of aeroelastic performance for Ting Kau Bridge Deck", *Wind Struct*., **4**(5), 367-382.

Cavagna, L., Quaranta, G. and Mantegazza, P. (2007), "Application of Navier-Stokes simulations for aeroelastic stability assessment in transonic regime", *Comput. Struct*., **85**(11-14), 818-832.

Gu, M. and Qin, X. (2004), "Direct identification of flutter derivatives and aerodynamic admittances of bridge decks", *Eng. Struct*., **26**(14), 2161-2172.

Kamakoti, R. and Shyy, W. (2004), "Fluid-structure interaction for aeroelastic applications", *Prog. Aerosp.Sci*., **40**(8), 535-558.

Tezduyar, E.T., Sathe, S., Pausewang, J., Schwaah, M., Christopher, J. and Crabtree J. (2008), " Interface projection techniques for fluid-structure interaction modeling with moving-mesh methods", *Comput. Mech*., **43**(1), 39-49.

Theodorsen, T. (1935), *General theory of aerodynamic instability and the mechanism of flutter, National Advisory Committee for Aeronautics (NACA)*, Washington, D.C., 1934, Technical Report.

Wang, Y. and Lin, Y. (2008), "Combination of CFD and CSD packages for fluid-structure interaction", *J. Hydrodynamics*, **20**(6), 756-761.

Zhiwen, Z., Zhaoxiang, W. and Zhengqing, C. (2008), "Computational fluid dynamic analyses of flutter characteristics for self-anchored suspension bridges", *Front. Archit. Civ. Eng. China*, **2**(3), 267-273.

King, J.P.C., Kong, L., Gómez-Martínez, R., Pozos-Estrada, A. and Sánchez-García R. (2011), "Experimental and analytical evaluation of the aeroelastic behaviour of the Baluarte bridge", *Proceedings of the 13th International Conference on Wind Engineering*, July 10-15.

Kim, S., Park, J., Kwon, S. and Kim, J. (2011), "Full scale monitoring of the 2nd Dolsan cable- stayed bridge during Typhoon Dianmu", *Proceedings of the 13th International Conference on Wind Engineering*, July 10-15.

Larsen, A. and Wall, A. (2011), "Shaping of bridge box girders of avoid vortex shedding response", *Proceedings*

of the 13th International Conference on Wind Engineering, July 10-15.

Larsen, S.V., Sinding, P. and Smitt, L.W. (2011), "Extraction of aerodynamic flutter derivatives in newly developed forced motion rig with 3 degrees of freedom", *Proceedings of the 13th International Conference on Wind Engineering*, July 10-15.

Mishra, S.S., Kumar, K. and Krishna, P. (2006), *Aeroelastic analysis of super long-span cablestayed bridges from flutter derivatives*, *Proceedings of the Advances in Bridge Engineering*.

Szabó, G. and Györgyi, J. (2009), "Three-dimensional fluid-structure interaction analysis for bridge aero-elasticity", *Proceedings of the World Congress on Engineering and Computer Science San Francisco*, USA, October 23-27.

Szabó, G. and Kristóf, G. (2010), "Three-dimensional numerical flutter simulation", *Proceedings of the 5th International Symposium on Computational Wind Engineering (CWE2010)*, Chapel Hill, USA, May 23-27.

Starossek, U. (1997), "Bridge flutter prediction with finite beam elements in complex notation", *Proceedings of the 7th International Conference on Computing in Civil and Building Engineering*, Seoul, Korea.

Xu, F.Y., Chen, A.R. and Ma, R.J. (2011), "Aeroelastic divergence research on Sutong Bridge", *Proceedings of the 13th International Conference on Wind Engineering*, July 10-15.

Zhu, L.D., Zhang, H. J., Guo, Z.S. and Hu, X.H. (2011), "Flutter performance and control measures of a 1400 m-span cable-stayed bridge scheme with steel box deck", *Proceedings of the 13th International Conference on Wind Engineering*, July 10-15.